The Astrophysical Journal Supplement Series, 237:8 (7pp), 2018 July https://doi.org/10.3847/1538-4365/aacc6a

Line Lists for AlF and AlCl in the $X^1\Sigma^+$ Ground State

Mahdi Yousefi[1] and Peter F. Bernath[1,2]
[1] Department of Physics, Old Dominion University, Norfolk, VA 23529-0126, USA; pbernath@odu.edu
[2] Department of Chemistry and Biochemistry, Old Dominion University, Norfolk, VA 23529-0126, USA
Received 2018 May 22; revised 2018 June 11; accepted 2018 June 11; published 2018 July 10

Abstract

Vibration-rotation line lists for AlF, $Al^{35}Cl$, and $Al^{37}Cl$ have been prepared in their ground electronic states ($X^1\Sigma^+$). Experimental rotational and ro-vibrational lines were employed to calculate a potential energy surface (PES) by direct potential fitting. The PES was used to calculate ro-vibrational energy levels. Born–Oppenheimer Breakdown corrections were included in the energy level calculations for AlCl. Ro-vibrational energy levels were calculated for the $v = 0$ to $v = 11$ vibrational levels and up to $J_{max} = 200$ for the rotational levels. Dipole moment functions covering the range of the PES turning points were calculated for AlCl and AlF by ab initio methods and used to determine line intensities. Partition functions for temperatures up to 3000 K were calculated. AlF and AlCl have been detected in circumstellar envelopes and are predicted to occur in cool stellar and sub-stellar atmospheres.

Key words: astronomical databases: miscellaneous – methods: laboratory: molecular – molecular data – opacity – techniques: spectroscopic

Supporting material: machine-readable tables

1. Introduction

AlF and AlCl are members of the aluminum monohalide family AlX (X = F, Cl, Br, I) and can be produced in the gas-phase by heating $AlCl_3$ or AlF_3 mixed with Al to high temperatures (Hedderich et al. 1993). AlCl also has been detected in a fast flow reactor from the reaction of Al with Cl_2 (Rogowski & Fontijn 1987). The $A^1\Pi$–$X^1\Sigma^+$ ultraviolet transition of AlCl has been observed in plumes produced by solid-fuel rockets (McGregor et al. 1993).

AlF and AlCl have astronomical importance. The rotational lines of AlF and AlCl have been detected in the circumstellar envelopes of carbon-rich stars such as IRC+10216 (Cernicharo & Guelin 1987; Ziurys & Apponi 1994; Agúndez et al. 2012). The major source of heavy elements in the interstellar medium is mass-loss from stellar winds associated with circumstellar shells of evolved stars. Understanding the physical and chemical processes in circumstellar envelopes helps our understanding of chemical abundances in the interstellar medium (Kwok 2007).

The existence of AlF and AlCl was predicted in C-rich and O-rich stellar atmospheres in thermal equilibrium calculations by Tsuji (1973). Although Tsuji (1973) did not consider condensation to form solids, he suggested that the lower temperature (~1000 K) calculations might apply to circumstellar envelopes. Detection of AlF and AlCl transitions by the IRAM 30 m radio telescope (Cernicharo & Guelin 1987) and the CSO telescope (Ziurys & Apponi 1994) supported Tsuji's suggestion (Cernicharo & Guelin 1987). In a detailed study, Agúndez et al. (2012) measured the molecular abundance of AlF and AlCl in the inner circumstellar layers of IRC+10216 and reported 1×10^{-8} and 7×10^{-8} relative abundances with respect to H_2 for AlF and AlCl, respectively. Agúndez et al. (2012) also found surprisingly high abundances in the cold outer shell of IRC+10216. Highberger et al. (2001) detected rotational transitions of AlF in the circumstellar envelope of CRL 2688, which is in a protoplanetary nebulae phase.

AlCl has also been observed in O-rich asymptotic giant branch (AGB) stars. Decin et al. (2017) reported the observation of AlCl in the circumstellar envelope of the red AGB stars R Dor and IK Tau in an attempt to identify Al-bearing species using the ALMA sub-millimeter telescope array.

There is also a possibility of detecting AlF and AlCl in the Sun's photosphere. Asplund et al. (2009) estimated the solar abundance of the elements and reported the abundances of 1.73×10^{-6}, 3.16×10^{-7}, and 3.63×10^{-8}, respectively, for Al, Cl, and F relative to H that makes the detection of AlF and AlCl possible in the Sun. Lodders & Fegley (2006) predicted the formation of AlF and AlCl in L- and T-type brown dwarfs below 2500 K.

Quantitative laboratory data are required to simulate the spectral energy distributions of astronomical objects (Bernath 2014). A reliable line list to calculate molecular opacities can be obtained through a combination of laboratory data and ab initio calculations. Mahieu et al. (1989) measured a high-resolution electronic spectrum of the $A^1\Pi$–$X^1\Sigma^+$ transition of AlCl. Hedderich et al. (1993) reported on high-resolution spectra of $Al^{35}Cl$ and $Al^{37}Cl$ up to $v = 8$ and $J = 167$. Wyse & Gordy (1972) measured rotational transitions of $Al^{35}Cl$ and $Al^{37}Cl$ in the millimeter region, and Hensel et al. (1993) measured microwave lines in a jet expansion.

Hedderich & Bernath (1992) recorded a high-resolution infrared spectrum of AlF with more than 500 ro-vibrational lines from bands with $v = 1 \rightarrow 0$ to $v = 5 \rightarrow 4$. Later, Zhang et al. (1995) extended the AlF ro-vibrational lines to higher J and v in order to obtain improved Dunham coefficients and an internuclear potential. Horiai & Uehara (2006) measured a ro-vibrational spectrum of the overtone band ($\Delta v = 2$) transitions of AlF between 1490 and 1586 cm^{-1} at high temperature with a diode laser spectrometer. Hoeft et al. (1970) used rotational transitions of AlF in the microwave region to determine Dunham coefficients.

Some other theoretical and experimental studies have been conducted in order to obtain dipole moments and dipole moment functions (DMFs). Lide (1965) studied the microwave transitions of gaseous AlF and AlCl at high temperature using a Stark spectrometer and determined the vibrationally averaged

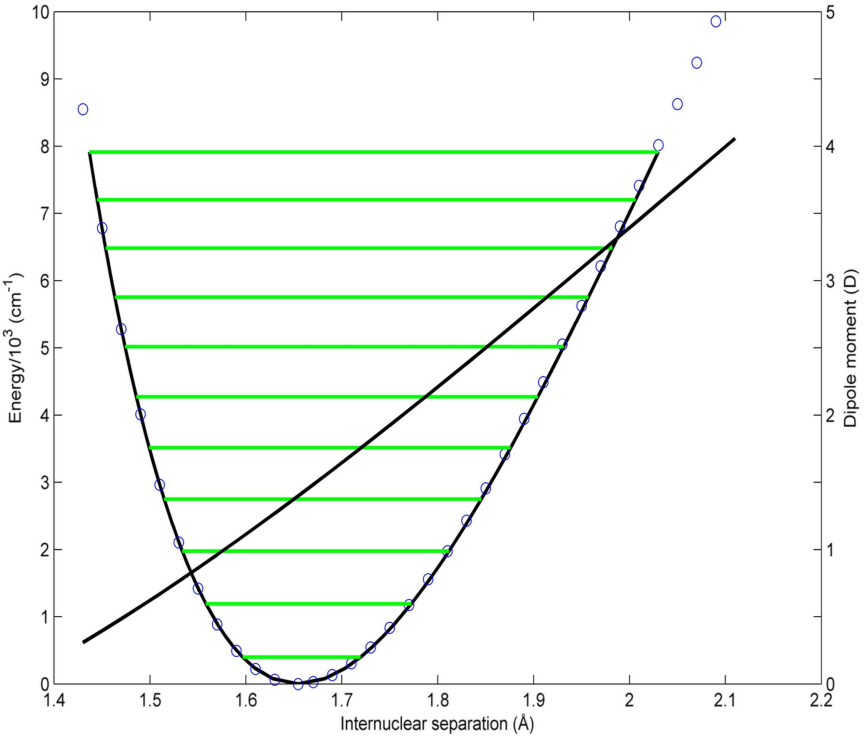

Figure 1. Potential energy surface of AlF calculated by RKR (—), PES from ab initio calculation (∘), and DMF (—)

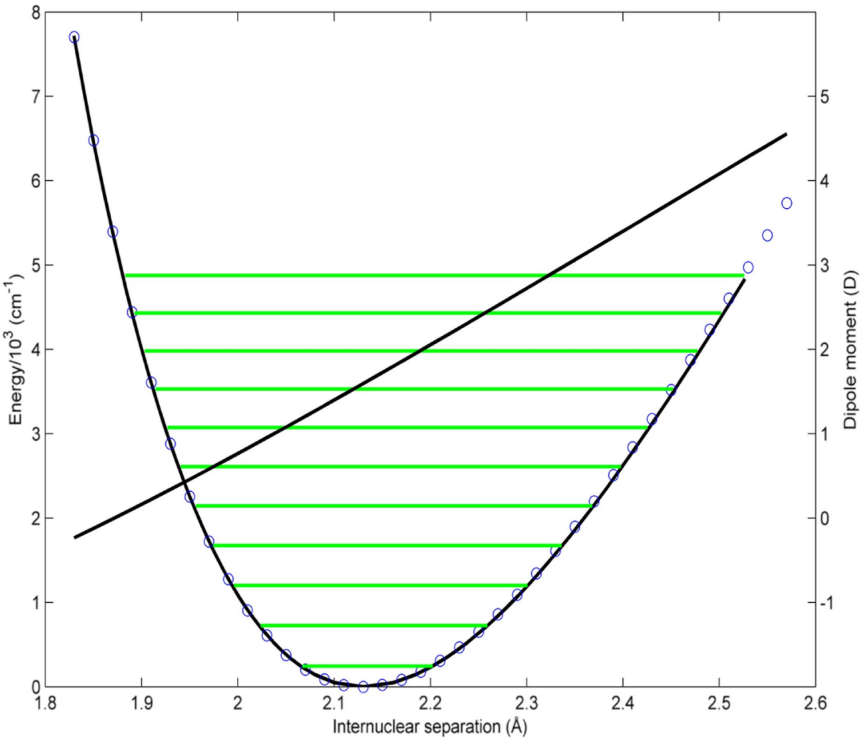

Figure 2. Potential energy surface of AlCl calculated by RKR (—), PES from ab initio calculation (∘), and DMF (—)

dipole moment for $v = 0$ of AlF to be 1.53 ± 0.1 debye (D); however, he did not report an AlCl dipole moment. Klein & Rosmus (1984) calculated a dipole of $\mu = 1.56$ D in the $v = 0$ vibrational level of AlF using the SCEP/CEPA method. Finally, Wan et al. (2016) computed the value of $\mu_e = 1.3087$ D as the permanent dipole moment for the $X^1\Sigma^+$ electronic state of AlCl at the equilibrium internuclear separation.

In this study we provide line lists for the ro-vibrational transitions of AlF and AlCl in their ground electronic states up to $v = 11$ and $J_{max} = 200$. Additionally, new ab initio DMFs

are computed for the $X^1\Sigma^+$ states of AlF and AlCl to provide line intensities.

2. Methods

2.1. Experimental Data

1100 high-resolution ro-vibrational and rotational lines of AlF from Zhang et al. (1995) and 1544 lines of $Al^{35}Cl$ and $Al^{37}Cl$ in the microwave and infrared regions from Hedderich et al. (1993) were used for the potential energy surface (PES) fitting. The observed lines of AlF are from $v = 0$ to $v = 9$, and J up to 101. The observed lines of $Al^{35}Cl$ are from $v = 0$ to $v = 8$, with a maximum J of 167 and $v = 0$ to $v = 5$, $J_{max} = 127$ for $Al^{37}Cl$.

2.2. DMF Calculations

Ab initio calculations have been performed using the Molpro 2012 package (Werner et al. 2012). The aug-cc-pwCV5Z basis set was used for DMF calculations. The active space includes (6 a_1, 3 b1, 3 b2, and 0 a_2) orbitals in the C_{2v} point group symmetry for both AlF and AlCl ab initio calculations. The calculations were performed using the average coupled-pair functional (ACPF) (Bauschlicher et al. 1990; Frohman et al. 2016) method. The wavefunction utilized for ACPF calculations were obtained by state-averaged CASSCF calculations. The dipole moment was calculated from 1.27 Å to 2.11 Å for AlF and from 1.77 Å to 2.61 Å for AlCl in 0.02 Å increments. The dipole moment points were calculated as an expectation value $\langle\psi|\mu(r)|\psi\rangle$ at a particular internuclear separation r.

2.3. PES and Ro-vibrational Energy Levels

PESs of AlF and AlCl were obtained by direct fitting of, respectively, 1100 and 1544 observed rotational and ro-vibrational frequencies of AlF and AlCl (Le Roy 2017a). Initially, Le Roy's RKR program (Le Roy 2017b) provided semi-classical turning points of the potential energy functions based on the Rydberg–Klein–Rees (RKR) procedure using experimentally determined rotational B_v and vibrational G_v constants. The RKR program generated turning points up to $v = 10$. Figures of the RKR PESs for the ground states of AlF and AlCl, including the ab initio potential surfaces and dipole moment points, for the $X^1\Sigma^+$ electronic states of AlF and AlCl, are presented in Figures 1 and 2, respectively. The RKR potentials have been used in Le Roy's Betafit program (Le Roy 2017c) to generate trial values of β_i for the Expanded Morse Oscillator (EMO) potential function using Equations (1)–(3):

$$V_{\rm EMO}(r) = D_e[1 - e^{-\beta(r)(r-r_e)}]^2, \quad (1)$$

$$\beta(r) = \beta_{\rm EMO}(y_q^{\rm ref}(r)) = \sum_{i=0}^{N_\beta} \beta_i y_q^{\rm ref}(r)^i, \quad (2)$$

$$y_q^{\rm ref}(r) = \frac{r^q - r_{\rm ref}^q}{r^q + r_{\rm ref}^q}. \quad (3)$$

The EMO potential was chosen for the fit because it requires a small number of adjustable parameters and extrapolates well (Barton et al. 2014). The dissociation energies of $D_e = 55564$ cm^{-1} and $D_e = 41653$ cm^{-1}, respectively, for AlF and AlCl, are taken from the literature (Hedderich et al. 1993) and are fixed in the fitting process. Le Roy's DPotfit program (Le Roy 2017a) was used to determine the empirical EMO potentials by least-squares fitting of the lines. Additionally, Born–Oppenheimer breakdown (BOB) corrections were included in the fit for AlCl to account for mass-dependent corrections for AlCl isotopologues. A detailed description of the Schrödinger equation, including the BOB adiabatic and non-adiabatic terms, is available in Le Roy (1999) and Le Roy & Huang (2002). The resulting parameters determined from DPotfit are r_e, β_i and BOB correction terms (u_i) with the corresponding fitting uncertainty for AlF and AlCl (Table 1).

Table 1
Fitting Parameters of the Empirical EMO Potentials for AlF and AlCl

Constants	AlF	AlCl
β_0	1.2998170(34)[a]	1.121878(31)
β_1	−0.591067(47)	−0.439891(88)
β_2	0.16823(43)	0.090230(54)
β_3	0.1256(48)	0.2068(75)
β_4	0.236(18)	−0.1030(36)
u_0^{Cl}	…	[0.00][b]
u_1^{Cl}	…	11.00(45)
u_2^{Cl}	…	−43(7.5)
u_∞^{Cl}	…	[0.00][b]
r_e/Å	1.654368(10)	2.1301672(50)
$D_e \times 10^{-4}$/cm^{-1}	[5.556402471][b]	[4.1653105][b]
σ_{rms}	0.719382	0.710634

Notes.
[a] Parameters were determined using sequential rounding and refitting procedure (Le Roy 1998).
[b] Values in squared brackets have been fixed during fitting.

Table 2
Dipole Moment Functions for the $X^1\Sigma^+$ States of AlF and AlCl in Debye

r/Å	AlF	AlCl
1.61	−1.171865525	…
1.65	−1.406679365	…
1.75	−1.93753402	…
1.85	−2.52118433	0.12302058
1.95	−3.125333165	−0.46020142
2.05	−3.742664015	−1.07884535
2.09	−3.991691835	−1.3341922
2.13	…	−1.59415822
2.17	…	−1.85543219
2.21	…	−2.12031688

(This table is available in its entirety in machine-readable form.)

3. Results and Discussion

3.1. DMF Evaluation

The point-wise ab initio DMFs were calculated for AlF and AlCl using the ACPF method as described in Section 2.2. The DMF points are provided in Table 2 for AlF and AlCl. The calculated equilibrium dipole moment values at bond lengths $r_e = 1.6543682$ and $r_e = 2.130143$ are $\mu_e = 1.406679$ and $\mu_e = 1.59415$ D, respectively, for AlF and AlCl.

To evaluate our DMF values, comparisons are made with values in the literature obtained from theory and experiments. Lide (1965) measured the microwave transitions of AlF and AlCl and obtained the value of $\mu_0 = 1.53 \pm 0.1$ D for the dipole moment of AlF. Later, Klein & Rosmus (1984) reported

Table 3
Calculated Band Transition Dipole Matrix Elements $R_{v''}^{v'}$ for the $X^1\Sigma^+$ State of AlF in D

v''	R_v^v	R_v^{v+1}	R_v^{v+2}	R_v^{v+3}	R_v^{v+4}	R_v^{v+5}
0	−1.43973	−0.235256	0.00898308	−0.0004441	3.31139E–05	−3.41133E–06
1	−1.50612	−0.335131	0.015849	−0.000905842	4.11727E–05	1.17658E–05
2	−1.57317	−0.413355	0.0227721	−0.00145677	6.67869E–05	9.75234E–06
3	−1.64089	−0.480586	0.0298703	−0.00212859	0.000111178	1.96783E–05
4	−1.70926	−0.540946	0.0371621	−0.00289252	0.000160964	0.000028645
5	−1.77826	−0.596479	0.0446437	−0.00376267	0.000228425	2.33072E–05
6	−1.84789	−0.648419	0.0523238	−0.00475932	0.000301221	2.76505E–05
7	−1.91812	−0.697573	0.0601758	−0.00586917	0.000401331	⋯
8	−1.98898	−0.744474	0.0682134	−0.00708091	⋯	⋯
9	−2.06044	−0.789498	0.0764442	⋯	⋯	⋯
10	−2.13247	−0.832954	⋯	⋯	⋯	⋯

Table 4
Calculated Band Transition Dipole Matrix Elements $R_{v''}^{v'}$ for the $X^1\Sigma^+$ State of $Al^{35}Cl$ in D

v''	R_v^v	R_v^{v+1}	R_v^{v+2}	R_v^{v+3}	R_v^{v+4}	R_v^{v+5}
0	−1.63011	−0.313273	0.0127291	−0.00066763	0.000027866	2.19962E–06
1	−1.7019	−0.444323	0.022221	−0.00135854	0.0000653217	4.94029E–06
2	−1.77398	−0.545726	0.0316667	−0.00218464	0.000119029	8.15688E–06
3	−1.84635	−0.631896	0.0411892	−0.00314095	0.000190878	1.12346E–05
4	−1.91901	−0.708389	0.050818	−0.00422295	0.000282796	1.41833E–05
5	−1.99193	−0.778046	0.0605625	−0.0054265	0.000396645	1.63401E–05
6	−2.06513	−0.842545	0.0704256	−0.00674889	0.000534418	1.70656E–05
7	−2.1386	−0.902974	0.0804076	−0.00818799	0.000697583	⋯
8	−2.21232	−0.960085	0.0905075	−0.00974247	⋯	⋯
9	−2.2863	−1.01442	0.100723	⋯	⋯	⋯
10	−2.36053	−1.0664	⋯	⋯	⋯	⋯

Table 5
Calculated Band Transition Dipole Matrix Elements $R_{v''}^{v'}$ for the $X^1\Sigma^+$ State of $Al^{37}Cl$ in D

v''	R_v^v	R_v^{v+1}	R_v^{v+2}	R_v^{v+3}	R_v^{v+4}	R_v^{v+5}
0	−1.62967	−0.311403	0.0125765	−0.000655516	2.71686E–05	2.14306E–06
1	−1.70061	−0.441656	0.0219525	−0.00133363	6.36417E–05	4.82234E–06
2	−1.77183	−0.542434	0.0312815	−0.00214419	0.000115906	7.99155E–06
3	−1.84333	−0.628064	0.0406849	−0.00308225	0.000185795	1.10357E–05
4	−1.91511	−0.704074	0.0501919	−0.00414334	0.00027515	0.000013986
5	−1.98716	−0.773287	0.0598119	−0.00532338	0.000385779	1.62065E–05
6	−2.05947	−0.83737	0.0695477	−0.00661968	0.000519618	1.71048E–05
7	−2.13205	−0.897406	0.0794	−0.00803011	0.000678101	⋯
8	−2.20488	−0.954143	0.0893676	−0.00955335	⋯	⋯
9	−2.27795	−1.00812	0.0994486	⋯	⋯	⋯
10	−2.35128	−1.05975	⋯	⋯	⋯	⋯

$\mu_0 = 1.65$ D as the vibrationally averaged dipole moment for the $v = 0$ of AlF using the coupled electron pair approximation (CEPA) and self-consistent electron pair approach (SCEP) methods. Wan et al. (2016) reported $\mu_0 = 1.3087$ D at equilibrium for the $X^1\Sigma^+$ state of AlCl.

Some of the vibrational transition dipole moment matrix elements (TDMMEs) for AlF from our calculation ($R_{v''}^{v'}$) are listed in Table 3. From this study (Table 3) the dipole moment for $v = 0$ is 1.44 D, which agrees with the value of, $\mu_0 = 1.53 \pm 0.1$ D derived by Lide (1965). As for AlF, we list some of the vibrational TDMMEs of $Al^{35}Cl$ and $Al^{37}Cl$ in Tables 4 and 5, respectively. The near linear form of the AlF and AlCl DMFs and the large first derivatives (Figures 1 and 2) lead to the noticeable decrease in TDMMEs from fundamental transitions to the overtone transitions (see Tables 3–5).

The equilibrium spectroscopic constants for AlF and AlCl were calculated using the PESs obtained from ab initio calculations. The calculated constants from this study, along with available constants from the literature obtained from experiments and theory, are presented in Table 6 for AlF and AlCl. By comparison with the experimentally derived equilibrium constants of AlF, the relative errors of calculated constants $\delta X/X$ with X = (r_e, ω_e, B_e, $\omega_e x_e$ and α_e) are respectively 0.04%, 0.50%, 0.09%, 2.60%, and 0.98% with respect to the experimentally measured equilibrium constants. The relative errors with respect to the experiments for the same constants for AlCl are 0.08%, 0.08%, 0.62%, 1.52%, and 0.84%. Overall, there is a good agreement between the calculated constants from this study, those listed in Table 6, and experimental values. In general, there is an improvement in the calculated equilibrium constants compared to other theoretical studies.

Table 6
Spectroscopic Parameters for the $X^1\Sigma^+$ States of AlF and AlCl Molecules

Molecule		r_e /Å	B_e/cm^{-1}	α_e /cm^{-1}	ω_e /cm^{-1}	$\omega_e x_e$/cm^{-1}	μ_e /D
AlF	This work	1.6536	0.552987	0.004935353	806.3542	4.72365	1.40668
	Reference (calc)[a]	1.664	0.546	0.005	805	4.3	1.543
	Expt.[b]	1.6543682	0.552480208	0.0049842	802.32	4.849	⋯
AlCl	This work	2.1283	0.2441156	0.0015974	484.8065	2.06968	1.59415
	Reference (calc)[c]	2.1374	0.2408	⋯	478.13	⋯	1.30866
	Reference (calc)[d]	2.146	⋯	⋯	467	⋯	⋯
	Reference (calc)[e]	2.140	0.2418	⋯	484.5	⋯	⋯
	Expt.[f]	2.13014336	0.24390066	0.001611082	481.7765	2.10181	⋯

Notes.
[a] Klein & Rosmus (1984).
[b] Hedderich & Bernath (1992).
[c] Wan et al. (2016).
[d] Langhoff et al. (1988).
[e] Brites et al. (2008).
[f] Hedderich et al. (1993).

Table 7
Line Lists of AlF, $Al^{35}Cl$, and $Al^{37}Cl$ in the $X^1\Sigma^+$ State

Isotopologue	Branch(J'')	v'	v''	$E_{v'',J''}$/cm^{-1}	$\tilde{\nu}$/cm^{-1}	$A_{J'\rightarrow J''}$/s^{-1}	$f_{J'\leftarrow J''}$	TDMMEs/D
AlF	R(30)	0	0	910.72614	33.9747	0.0128331	1.72143E–05	−1.4562
AlF	R(30)	1	0	910.72614	821.75425	4.65744	1.0679E–05	−0.233211
AlF	P(35)	1	0	1091.46653	748.48055	3.86434	1.00499E–05	−0.240689
AlF	R(30)	1	1	1698.81235	33.66805	0.0136604	1.86593E–05	−1.52298
AlF	R(30)	2	1	1698.81235	811.95803	9.10694	2.13882E–05	−0.332028
AlF	P(35)	2	1	1877.92073	739.34407	7.56665	2.01678E–05	−0.343061
AlF	R(30)	3	2	2477.40681	802.27935	13.3499	3.21141E–05	−0.409297
AlF	P(35)	3	2	2654.89475	730.32055	11.1077	3.03421E–05	−0.423381
$Al^{35}Cl$	R(30)	0	0	466.34315	15.044	0.00141992	9.71417E–06	−1.6439
$Al^{35}Cl$	R(30)	1	0	466.34315	491.04991	1.77495	1.13973E–05	−0.311668
$Al^{35}Cl$	P(35)	1	0	546.39396	458.71304	1.54233	1.06793E–05	−0.316932
$Al^{35}Cl$	R(30)	1	1	942.4483	14.94475	0.00151654	1.05134E–05	−1.71586
$Al^{35}Cl$	R(30)	2	1	942.4483	486.8156	3.47679	2.27153E–05	−0.441907
$Al^{35}Cl$	P(35)	2	1	1021.9708	454.69188	3.02373	2.13087E–05	−0.449661
$Al^{35}Cl$	R(30)	3	2	1414.41783	482.62055	5.10716	3.39497E–05	−0.542587
$Al^{35}Cl$	P(35)	3	2	1493.41525	450.70873	4.4455	3.18843E–05	−0.552466
$Al^{37}Cl$	R(30)	0	0	458.2026	14.69132	0.00132114	9.47754E–06	−1.64313
$Al^{37}Cl$	R(30)	1	0	458.2026	485.15124	1.69151	1.11273E–05	−0.30982
$Al^{37}Cl$	P(35)	1	0	536.37728	453.5759	1.47282	1.04303E–05	−0.314984
$Al^{37}Cl$	R(30)	1	1	928.7583	14.59555	0.00141002	1.02483E–05	−1.71423
$Al^{37}Cl$	R(30)	2	1	928.7583	481.0168	3.3142	2.21782E–05	−0.439276
$Al^{37}Cl$	P(35)	2	1	1006.42323	449.64712	2.88814	2.08124E–05	−0.44688
$Al^{37}Cl$	R(30)	3	2	1395.27478	476.92024	4.86958	3.31489E–05	−0.539343
$Al^{37}Cl$	P(35)	3	2	1472.4329	445.75504	4.24716	3.11426E–05	−0.549028

(This table is available in its entirety in machine-readable form.)

3.2. Line List

The PESs from Le Roy's DPotfit program with the ab initio DMFs have been used in Le Roy's LEVEL program (Le Roy 2017d). LEVEL generates ro-vibrational energy levels by solving a one-dimensional Schrödinger equation and provides vibrational transition matrix elements $\langle\psi_{v'J'}|\mu(r)|\psi_{v''J''}\rangle$ that depend on J and therefore account for the Herman–Wallis effect (Herman & Wallis 1955). Additionally, LEVEL calculates Einstein A coefficients in s^{-1} units by (Bernath 2016):

$$A_{J'\rightarrow J''} = \frac{16\pi^2\nu^3 S_{J''}^{\Delta J}}{3\varepsilon_0 hc^3(J'+1)} |\langle\psi_{v',J'}|\mu(r)|\psi_{v'',J''}\rangle|^2, \quad (4)$$

where ν is the frequency, $S_{J''}^{\Delta J}$ is the Hönl–London factor, and $\mu(r)$ is the DMF. The oscillator strengths $f_{J'\leftarrow J''}$, have been calculated from Einstein A coefficients by (Bernath 2016)

$$f_{J'\leftarrow J''} = 1.4991938\frac{1}{\tilde{\nu}^2}\frac{(2J'+1)}{(2J''+1)}A_{J'\rightarrow J''}, \quad (5)$$

where $\tilde{\nu}$ is the transition wavenumber in cm^{-1}.

We present a line list of AlF, $Al^{35}Cl$, and $Al^{37}Cl$ in their ground states. The line lists for AlF, $Al^{35}Cl$, and $Al^{37}Cl$ are calculated up to $v = 11$ and $J = 200$ and are provided in Table 7. The line list calculations with transitions up to $\Delta v = 5$ were included for AlF and AlCl. We note that for $\Delta v > 5$ the

Table 8
Partition Functions for AlF and AlCl Isotopologues in the $X^1\Sigma^+$ State

T(K)	AlF[a]	AlF[b]	AlF[c]	$Al^{35}Cl$[a]	$Al^{35}Cl$[b]	$Al^{35}Cl$[c]	$Al^{37}Cl$[a]	$Al^{37}Cl$[b]	$Al^{37}Cl$[c]
9.375	73.121	73.121	73.121	651.305	651.313	651.312	666.782	666.7812	666.784
18.75	144.197	144.197	144.197	1294.595	1294.603	1294.605	1325.547	1325.547	1325.553
37.5	286.394	286.394	286.395	2581.433	2581.441	2581.450	2643.340	2643.340	2643.353
75	570.878	570.878	570.881	5156.529	5155.992	5156.014	5280.443	5279.821	5279.848
150	1140.736	1140.162	1140.167	10415.973	10308.525	10308.574	10672.472	10556.298	10556.350
225	1720.786	1709.861	1709.868	16237.658	15465.635	15465.709	16658.336	15837.462	15837.536
300	2341.067	2279.975	2279.982	22973.382	20627.343	20627.220	23598.714	21123.334	21123.137
375	2995.161	⋯	⋯	30765.028	⋯	⋯	31636.892	⋯	⋯
425	3470.974	⋯	⋯	36576.162	⋯	⋯	37635.798	⋯	⋯
500	4241.029	⋯	⋯	46240.958	⋯	⋯	47617.523	⋯	⋯
575	5082.399	⋯	⋯	57060.518	⋯	⋯	58796.526	⋯	⋯
650	5997.727	⋯	⋯	69048.751	⋯	⋯	71186.951	⋯	⋯
725	6988.727	⋯	⋯	82216.802	⋯	⋯	84800.200	⋯	⋯
800	8056.609	⋯	⋯	96574.498	⋯	⋯	99646.370	⋯	⋯
875	9202.296	⋯	⋯	112131.018	⋯	⋯	115734.917	⋯	⋯
925	10009.692	⋯	⋯	123172.426	⋯	⋯	127155.347	⋯	⋯
1000	11286.688	⋯	⋯	140746.595	⋯	⋯	145334.771	⋯	⋯
1250	16121.530	⋯	⋯	208202.814	⋯	⋯	215130.344	⋯	⋯
1500	21860.979	⋯	⋯	289563.110	⋯	⋯	299333.846	⋯	⋯
1750	28523.818	⋯	⋯	385161.775	⋯	⋯	398291.300	⋯	⋯
2000	36128.794	⋯	⋯	495347.356	⋯	⋯	512363.320	⋯	⋯
2250	44695.105	⋯	⋯	620483.981	⋯	⋯	641926.102	⋯	⋯
2500	54242.599	⋯	⋯	760950.631	⋯	⋯	787370.039	⋯	⋯
2750	64791.894	⋯	⋯	917138.157	⋯	⋯	949095.786	⋯	⋯
3000	76364.465	⋯	⋯	1089444.116	⋯	⋯	1127507.992	⋯	⋯

Notes.
[a] Calculated partition function including quasibound levels.
[b] Calculated partition function for the $v = 0$ vibrational level.
[c] Calculated partition function from the JPL database.

Table 9
Polynomial Coefficients Determined from Regression of Equation (7)

Polynomial coefficient	AlF	$Al^{35}Cl$	$Al^{37}Cl$
a_0	0.4854277	4.1929305	4.2530758
a_1	2.9113006	−6.4086498	−6.5837492
a_2	−3.3592917	9.1230438	9.3668437
a_3	2.8840883	−5.5849132	−5.7569906
a_4	−1.2934446	1.7766208	1.8414362
a_5	0.2877944	−0.2764733	−0.2888155
a_6	−0.0246505	0.016656	0.0175889

calculated band intensities no longer decrease as expected (Medvedev et al. 2016) and are therefore excluded.

3.3. Partition Function

The partition functions have been calculated for AlF, $Al^{35}Cl$, and $Al^{37}Cl$ with vibrational levels up to the dissociation limit including quasibound levels by

$$Q = \sum_{v=0}^{v_{\max}} \left(\sum_{J=0}^{J_{\max}} (2J+1) e^{-\frac{E_{v,J}}{kT}} \right). \quad (6)$$

The partition functions have been calculated for temperatures up to $T = 3000$ K with 75 K increments up to 1000 K and increasing by 250 K increments up to 3000 K, including temperatures available in the JPL database (Pickett 1991). As a check, the partition functions for $v = 0$ were calculated and included for comparison purposes with the available partition functions in the JPL database. Partition functions including those from the JPL database are presented in Table 8 for AlF, $Al^{37}Cl$, and $Al^{35}Cl$. The calculated partition functions from our study agree well with those in the JPL database. Polynomial fits of the partition functions of AlF, $Al^{37}Cl$, and $Al^{35}Cl$ have been performed using the following expression and the determined a_n coefficients are provided in Table 9:

$$\log_{10} Q = \sum_{n=0}^{n_{\max}} a_n (\log_{10} T)^n . \quad (7)$$

4. Conclusions

EMO empirical potentials for AlF, $Al^{35}Cl$, and $Al^{37}Cl$ have been determined by direct potential fitting using observed vibrational and rotational transitions. Additionally, an ab initio DMF calculations were performed for AlF and AlCl. Line lists of AlF, $Al^{35}Cl$, and $Al^{37}Cl$ in their $X^1\Sigma^+$ ground state have been calculated using ab initio DMF and the fitted potential. The line lists can be used to compute molecular opacities for AlF and AlCl.

This work was supported by NASA Exoplanet grant NNX16AB51G. We thank A. Fernando for some initial work on AlF.

Software: Molpro 2012 (Werner et al. 2012), dPotfit 2017 (Le Roy 2017a), RKR1 2017 (Le Roy 2017b), betaFIT 2017 (Le Roy 2017c), LEVEL 2017 (Le Roy 2017d).

ORCID iDs

Peter F. Bernath https://orcid.org/0000-0002-1255-396X

References

Agúndez, M., Fonfría, J. P., Cernicharo, J., et al. 2012, A&A, 543, A48
Asplund, M., Grevesse, N., Sauval, A. J., & Scott, P. 2009, ARAA, 47, 481
Barton, E. J., Chiu, C., Golpayegani, S., et al. 2014, MNRAS, 442, 1821
Bauschlicher, Jr., C. W., Langhoff, S. R., & Komornicki, A. 1990, AcTC, 77, 263
Bernath, P. F. 2014, RSPTA, 372, 20130087
Bernath, P. F. 2016, Spectra of Atoms and Molecules (3rd ed.; Oxford: Oxford Univ. Press)
Brites, V., Hammoutène, D., & Hochlaf, M. 2008, JPCA, 112, 13419
Cernicharo, J., & Guelin, M. 1987, A&A, 183, 10
Decin, L., Richards, A. M. S., Waters, L. B. F. M., et al. 2017, A&A, 608, A55
Frohman, D. J., Bernath, P. F., & Brooke, J. S. A. 2016, JQSRT, 169, 104
Hedderich, H. G., & Bernath, P. F. 1992, JMoSp, 153, 73
Hedderich, H. G., Dulick, M., & Bernath, P. F. 1993, JChPh, 99, 8386
Hensel, K. D., Styger, C., Jäger, W., Merer, A. J., & Gerry, M. C. L. 1993, JChPh, 99, 3320
Herman, R., & Wallis, R. F. 1955, JChPh, 23, 637
Highberger, J. L., Savage, C., Bieging, J. H., & Ziurys, L. M. 2001, ApJ, 562, 790
Hoeft, J., Lovas, F., Tiemann, E., & Törring, T. 1970, ZNatA, 25, 1029
Horiai, K., & Uehara, H. 2006, AcSpA, 1009, 1012
Klein, R., & Rosmus, P. 1984, Theoret. Chim. Acta, 66, 21
Kwok, S. 2007, Physics and Chemistry of the Interstellar Medium (Mill Valley, CA: Univ. Science Books)
Langhoff, S. R., Bauschlicher, C. W., Jr, & Taylor, P. R. 1988, JChPh, 88, 5715
Le Roy, R. J. 1998, JMoSp, 191, 223
Le Roy, R. J. 1999, JMoSp, 194, 189
Le Roy, R. J. 2017a, JQSRT, 186, 179
Le Roy, R. J. 2017b, JQSRT, 186, 158
Le Roy, R. J. 2017c, JQSRT, 186, 210
Le Roy, R. J. 2017d, JQSRT, 186, 167
Le Roy, R. J., & Huang, Y. 2002, JMoSt (Theochem), 591, 175
Lide, D. R., Jr 1965, JChPh, 42, 1013
Lodders, K., & Fegley, B. 2006, Astrophysics Update 2: Chemistry of Low Mass Substellar Objects (Berlin: Springer)
Mahieu, E., Dubois, I., & Bredohl, H. , 1989, JMoSp, 134, 317
McGregor, W. K., Drakes, J. A., Beale, K. S., & Sherrell, F. G. 1993, JTHT, 7, 736
Medvedev, E. S., Meshkov, V. V., Stolyarov, A. V., Ushakov, V. G., & Gordon, I. E. 2016, JMoSp, 330, 36
Pickett, H. M. 1991, JMoSp, 148, 371
Rogowski, F., & Fontijn, A. 1987, CPL, 137, 219
Tsuji, T. 1973, A&A, 23, 411
Wan, M., Yuan, D., Jin, C., et al. 2016, JChPh, 145, 024309
Werner, H. J., Knowles, P. J., Knizia, G., Manby, F. R., & Schütz, M. 2012, Comput. Mol. Sci., 2, 242
Wyse, F. C., & Gordy, W. 1972, JChPh, 56, 2130
Zhang, K. Q., Guo, B., Braun, V., Dulick, M., & Bernath, P. F. 1995, JMoSp, 170, 82
Ziurys, L. M., & Apponi, A. J. 1994, ApJ, 433, 729